J. Fluid Mech. (1999), *vol.* 397, *pp.* 331–349. Printed in the United Kingdom

Surface shear viscosity of Gibbs and Langmuir monolayers

By CATHERINE BARENTIN, CHRISTOPHE YBERT†, JEAN-MARC DI MEGLIO‡ AND JEAN-FRANÇOIS JOANNY

Institut Charles Sadron (CNRS UPR 022), 6 rue Boussingault, 67083 Strasbourg Cedex, France

(Received 22 December 1998 and in revised form 21 June 1999)

In this paper, we present a new two-dimensional viscometer, and the hydrodynamic calculations used to obtain the surface viscosities from the measurements. In order to interpret the experiments, performed with solutions of sodium dodecyl sulfate (SDS) and also with monolayers of insoluble surfactants, we develop various hydrodynamic models of soluble Gibbs monolayers and of incompressible Langmuir monolayers, that describe well the experimental results. In the case of SDS solutions, the calculations allow the determination of the surface shear viscosity, and its value is in good agreement with previous studies.

1. Introduction

The surface shear viscosity of adsorbed surfactant or polymer monolayers plays a crucial role in many dynamic processes at fluid interfaces, such as the formation, stability and rheology of emulsions and foams. It is also relevant for industrial processes involving film coating, flotation or oil recovery (see Malhotra & Wasan 1988). Various types of viscometers (see Edwards, Brenner & Wasan 1991) have been developed to measure surface viscosities; the most widely used is the deep-channel viscometer (with a sensitivity of order 10^{-7} Pa m s according to Mannheimer & Schechter 1970), where one measures the flow through a channel created by a surface pressure gradient; the rotating wall knife-edge viscometer has a sensitivity of order 10^{-8} Pa m s. The main drawback of these two techniques is the use of tracer particles, which are introduced in the monolayers in order to visualize the velocity field or the rotation period. Other devices such as the rotating disk avoid this problem, but are less sensitive (10^{-5} Pa m s). Recently, Danov *et al.* (1995) and Petkov, Danov & Denkov (1996) have developed an original method: they measure the drag coefficient of a small particle partially immersed in the subphase. Their method is sensitive and it does not make use of any tracers, but the determination of the surface viscosity from the measurements requires numerical resolution of the hydrodynamic equations. In this paper, we present a new viscosimeter, based on the same principle: we measure the drag force acting on a macroscopic disk translating in a viscous surface layer and overlaying a subphase of finite depth. The simpler geometry allows an analytical solution of the hydrodynamic problem.

In other respects, a thin disk lying in a viscous sheet is the macroscopic analogue of

† Present address: Laboratoire de dynamique des fluides complexes (UMR 7506 ULP–CNRS), Institut de physique, 3 rue de l'Université, 67084 Strasbourg Cedex, France.
‡ Member of the Institut Universitaire de France.

biological systems such as proteins or lipids incorporated into membranes (Saffman & Delbruck 1975). Protein diffusion within bilayers has been the subject of a variety of theoretical treatments. The first hydrodynamic model was proposed by Saffman (1976), who treats the rotation and the translation of a thin disk in a viscous sheet overlaying a subphase of infinite depth. Saffman calculated, in the limit of large viscosities, an approximate solution for the drag force acting on the disk. This model was later extended by Hughes, Pailthorpe & White (1981), who gave the general expression for the force at any viscosity. The applicability of this model to the diffusion of proteins or lipids in membranes was analysed in Vaz *et al.* (1987) and Clegg & Vaz (1985). More recently, Evans & Sackmann (1988) studied the influence of the finite thickness of the water substrate on the motion of the disk. They imposed a proportionality between the velocity and the shear stress exerted by the subphase on the membrane and they calculated the force acting on the disk overlying a subphase of finite depth. In their model, the subphase depth is small compared to the disk radius. Stone & Ajdari (1998) have generalized these results to any value of subphase depth, using numerical calculations; they have also studied the range of validity of the Evans–Sackmann formula.

In this paper, we use the same geometry as Evans & Sackmann, but we explicitly calculate the shear stress and the drag force using the lubrication approximation, which allows an explicit analytical resolution. We study both the case of an incompressible Langmuir (insoluble) monolayer (we find the same expression for the force as that given in Evans & Sackman 1988) and the case of a Gibbs (soluble) monolayer for which we obtain new results. Soluble monolayers were previously studied by Danov *et al.* (1995) but in a different geometry and with numerical methods. The results on insoluble monolayers are used to interpret experiments with insoluble surfactants and polymers; the results on soluble monolayers describe the behaviour of monolayers of soluble surfactants. For those monolayers, especially in the case of polymer monolayers, the surface viscosity may depend on frequency. In this paper, we only consider the behaviour at zero frequency; we therefore do not study the viscoelastic response.

From a pure theoretical viewpoint this system is also interesting, since it reveals the importance of the coupling between the surface layer and the subphase. Indeed this coupling allows a solution of the two-dimensional Stokes equation, which satisfies all the boundary conditions. This important point was understood first by Saffman, who showed that the bidimensional motion of membrane-trapped particles induces flow fields in the surrounding medium, which exert a reaction force on the surface layer. The underlying bulk layer exerts a drag force and screens the surface velocity field. This eliminates the logarithmic divergence of the velocity field in a pure bidimensional motion.

The paper is organized as follows: we first study the hydrodynamics and calculate the force acting on the thin disk in cases of both an insoluble and a soluble viscous monolayer. In § 3, the experimental device is presented and the results obtained on several systems are compared with the predicted forces. This comparison gives a measure of the various viscosities. Finally, we discuss possible improvements of the experimental device and we give some perspectives.

2. Forces acting on a translating thin disk

2.1. *Hydrodynamic equations*

We consider the problem sketched on figure 1. A disk of radius R moves at constant velocity $\boldsymbol{U}$ along the surface. The subphase has a finite depth h in the z-direction

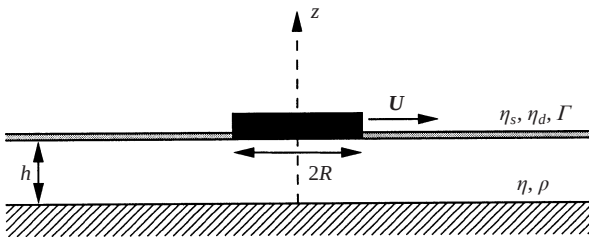

FIGURE 1. Parameters of the hydrodynamic model: a disk moves at constant velocity $\boldsymbol{U}$ in a viscous sheet, overlaying a subphase of finite depth h.

and is infinite in the perpendicular directions. The depth h is small compared to the radius of the disk R. In this section, we determine the velocity field in the subphase. We denote by $\boldsymbol{v} = (v_r, v_\theta, v_z)$, the velocity in the subphase and by P the pressure field; we use cylindrical coordinates. We assume that a stationary state is reached. The subphase is treated as an incompressible fluid and the hydrodynamic equations are the Stokes and the continuity equations:

$$\eta \nabla^2 \boldsymbol{v} = \nabla P \quad \text{and} \quad \nabla \cdot \boldsymbol{v} = 0. \tag{2.1a,b}$$

The boundary conditions on the velocity are the no-slip conditions at the surface $z = h$ and at the bottom of the subphase $z = 0$:

$$\left.\begin{aligned} \boldsymbol{v}(r, \theta, 0) &= \boldsymbol{0}, \\ \boldsymbol{v}(r, \theta, h) &= \boldsymbol{u}_s(r, \theta), \end{aligned}\right\} \tag{2.2}$$

where $\boldsymbol{u}_s$ is the velocity of the surface. We now use the lubrication approximation: we neglect the vertical component of the velocity v_z compared to the horizontal components and we ignore the vertical pressure gradient $\partial P / \partial z$. This assumption remains valid as long as h is smaller than any horizontal characteristic length scale of the velocity field. Under these conditions, the Stokes equation reduces to

$$\eta \frac{\partial^2 \boldsymbol{v}_{\shortparallel}}{\partial z^2} = \nabla_s P \tag{2.3}$$

where $\boldsymbol{v}_{\shortparallel}$ is the velocity parallel to the surface. This last equation is integrated, taking account of the boundary conditions:

$$\boldsymbol{v}(r, \theta, z) = \frac{(z^2 - zh)}{2\eta} \nabla_s P(r, \theta) + \frac{z}{h} \boldsymbol{u}_s(r, \theta). \tag{2.4}$$

From (2.4), the shear stress at the upper surface can be calculated:

$$\boldsymbol{\sigma}_t = -\eta \left.\frac{\partial \boldsymbol{v}}{\partial z}\right|_{z=h} = -\frac{h}{2} \nabla_s P - \eta \frac{\boldsymbol{u}_s}{h} \tag{2.5}$$

where $\boldsymbol{\sigma}_t$ is the projection of the stress tensor on the z-axis (i.e. the force per unit area exerted by the subphase on the surface layer). An other important quantity is the average velocity defined by

$$\boldsymbol{V} = \frac{1}{h} \int_0^h \boldsymbol{v}_{\shortparallel}(z)\, \mathrm{d}z. \tag{2.6}$$

Using the continuity equation and the boundary conditions on the velocity, it is easy to show, that $\nabla_s \cdot \boldsymbol{V} = 0$. This leads to a useful relation:

$$\nabla_s \cdot \boldsymbol{u}_s = \frac{h^2}{6\eta} \nabla_s^2 P. \tag{2.7}$$

Equation (2.7) implies that $\nabla_s^2 P$ does not vanish for a compressible surface layer. This appears surprising at first sight, as $\nabla^2 P = 0$, and $\partial P/\partial z$ is negligible compared to $\partial P/\partial x$. However, in Appendix A, we show that the second derivative with respect to z of the pressure is of the same order of magnitude as the other second derivatives with respect to x, y.

2.2. *Incompressible viscous monolayer*

We denote by $\boldsymbol{u}_s(r, \theta)$, Π_s the surface velocity and the surface pressure, respectively, and by η_s the bidimensional analogue of the viscosity. Dimensionally, η_s is homogeneous to a viscosity times a length. The Stokes equation, applied to the surface layer, reads

$$\eta_s \nabla_s^2 \boldsymbol{u}_s - \nabla_s \Pi_s + \boldsymbol{\sigma}_t = \boldsymbol{0} \tag{2.8}$$

and the boundary conditions are

$$\left.\begin{aligned} \boldsymbol{u}_s(r = R, \theta) &= \boldsymbol{U}, \\ \lim_{r\to\infty} \boldsymbol{u}_s &= \boldsymbol{0}, \\ \lim_{r\to\infty} \Pi_s &= 0. \end{aligned}\right\} \tag{2.9}$$

We look for stationary solutions depending only on r and θ. The symmetry of the problem imposes the following form of the surface velocity field:

$$\boldsymbol{u}_s \left| \begin{array}{l} u_{s,r}(r, \theta) = U f(r) \cos\theta \\ u_{s,\theta}(r, \theta) = -U g(r) \sin\theta \end{array} \right. \tag{2.10}$$

where f and g are yet unknown functions.

2.2.1. *Subphase pressure*

For an incompressible surface layer, the velocity obeys $\nabla_s \cdot \boldsymbol{u}_s = 0$. This equation combined with (2.7) imposes that $\nabla_s^2 P = 0$. In this case, the pressure can be considered as independent of the height z and in order to respect the symmetry, it is written as $P = h(r) \cos\theta$. We obtain

for $r < R$: $P(r, \theta) = Ar \cos\theta$,

for $r > R$: $P(r, \theta) = B/r \cos\theta$.

The continuity of the velocity and the shear stress (2.5), at $r = R$, implies that the pressure gradient is also continuous. Taking account of the continuity of P and $\nabla_s P$, at $r = R$ we find $A = B = 0$. This result is in agreement with those found by Hughes *et al.* (1981) and Stone & Ajdari (1998). The pressure is uniform in the subphase and the shear stress reduces to $\boldsymbol{\sigma}_t = -\eta \boldsymbol{u}_s/h$. This results from a simple shear flow.

2.2.2. *Surface flow field*

For an incompressible surface layer, the Stokes and the continuity equations read

$$\eta_s \nabla_s^2 \boldsymbol{u}_s - \nabla_s \Pi_s - \frac{\eta \boldsymbol{u}_s}{h} = \boldsymbol{0} \quad \text{and} \quad \nabla_s \cdot \boldsymbol{u}_s = 0. \tag{2.11a,b}$$

To solve this system of equations, we take respectively the divergence and the curl of (2.11*a*); we obtain a system of decoupled equations for the surface pressure and the

curl of the velocity:

$$\nabla_s^2 \Pi_s = 0, \tag{2.12a}$$

$$(\nabla_s^2 - \kappa^2)\nabla_s \times \boldsymbol{u}_s = \boldsymbol{0} \quad \text{with} \quad \kappa^2 = \frac{\eta}{h\eta_s}. \tag{2.12b}$$

The inverse length κ is an important parameter of the problem. In fact, κ^{-1} is the characteristic length scale of the velocity decay; we call it the hydrodynamic screening length. Far away from the disk, the velocity decreases exponentially over a distance κ^{-1}. This new length imposes another condition for the validity of the lubrication approximation: $\kappa^{-1} \gg h$ or equivalently $\eta_s \gg \eta h$.

The curl of the velocity, satisfying (2.12*b*), is a linear combination (Abramowitz & Stegun 1984) of the modified Bessel functions of order one K_1 and I_1, but due to the fact that the velocity decays to zero at infinity, we obtain

$$\nabla_s \times \boldsymbol{u}_s = C_1 U K_1(\kappa r) \sin\theta \, \boldsymbol{e}_z. \tag{2.13}$$

Equation (2.12*a*) together with the symmetry of the problem then imposes

$$\Pi_s = \frac{M \cos\theta}{r}. \tag{2.14}$$

C_1 and M are integration constants.

The velocity field and the surface pressure are obtained by integration from (2.13), and by imposing the continuity of both components of the surface velocity at the edge of the disk ($r = R$):

$$\boldsymbol{u}_s = U \left| \begin{array}{c} \left(\dfrac{R^2}{r^2} \dfrac{K_2(\kappa R)}{K_0(\kappa R)} + \dfrac{K_2(\kappa r) - K_0(\kappa r)}{K_0(\kappa R)} \right) \cos\theta \\ -\left(-\dfrac{R^2}{r^2} \dfrac{K_2(\kappa R)}{K_0(\kappa R)} + \dfrac{K_0(\kappa r) + K_2(\kappa r)}{K_0(\kappa R)} \right) \sin\theta \end{array} \right. \tag{2.15}$$

and

$$\Pi_s = \frac{\eta U}{h} \frac{R^2}{r} \frac{K_2(\kappa R)}{K_0(\kappa R)} \cos\theta. \tag{2.16}$$

2.2.3. *Total force on the disk*

The force acting on the disk has two contributions. The first contribution is the drag force due to the subphase:

$$\boldsymbol{F}_{\text{sub.}} = \pi R^2 \boldsymbol{\sigma}_t = -\pi R^2 \frac{\eta}{h} \boldsymbol{U}. \tag{2.17}$$

The second one is the force exerted by the thin surface layer on the perimeter of the disk, $\boldsymbol{F}_{\text{surf.}} = \int_0^{2\pi} R(\sigma_{rr}\boldsymbol{e}_r + \sigma_{r\theta}\boldsymbol{e}_\theta)\,\mathrm{d}\theta$. The components σ_{ij} of the two-dimensional stress are given by $\sigma_{rr} = -\Pi_s + 2\eta_s \partial u_{s,r}/\partial r$ and $\sigma_{r\theta} = \eta_s \left(\partial u_{s,r}/r\partial\theta + r\partial(u_{s,\theta}/r)/\partial r \right)$ taken at $r = R$. Using the expressions for the velocity and the surface pressure (2.15), (2.16), we obtain

$$\boldsymbol{F}_{\text{surf.}} = -\frac{\pi R^2 \eta}{h} \left(2\frac{K_2(\kappa R)}{K_0(\kappa R)} - 1 \right) \boldsymbol{U} \tag{2.18}$$

so that the total force, $\boldsymbol{F}_{\text{tot.}} = \boldsymbol{F}_{\text{sub.}} + \boldsymbol{F}_{\text{surf.}}$ is equal to

$$\boldsymbol{F}_{\text{tot.}} = -\frac{2\pi R^2 \eta}{h} \frac{K_2(\kappa R)}{K_0(\kappa R)} \boldsymbol{U}. \tag{2.19}$$

It is the same expression as found by Evans & Sackmann (1988), who did not calculate explicitly the shear stress $\boldsymbol{\sigma}_t$; they only imposed the proportionality between the shear stress and the local velocity: $\boldsymbol{\sigma}_t = b_s \boldsymbol{u}_s$. More recently, Stone & Ajdari computed numerically the force acting on the disk for any value of the subphase depth and they studied the range of validity of the Evans–Sackmann formula. They showed that the force (2.19) provides an excellent approximation for $\kappa^{-1} > h$ and $\kappa^{-2} > hR$ and that the lubrication approximation is accurate provided that $h/R < 0.2$.

In the limit of large viscosities, where the lubrication approximation is legitimate, the characteristic distance κ^{-1} diverges. The asymptotic behaviour of the force is found by replacing κ^{-1} by the lateral size of the monolayer L. The force tends to

$$\boldsymbol{F}_{\text{tot.}} \sim -\frac{4\pi\eta_s}{\ln(L/R) + \ln(1/2)} \boldsymbol{U}. \tag{2.20}$$

This expression is in agreement with the result presented in Happel & Brenner (1991), where the force per unit length acting on an infinite cylinder translating in a viscous fluid between two planes a distance L apart is calculated: the same logarithmic dependence on the cylinder size is found. (This dependence comes from the fact that the influence of the subphase vanishes in the limit of large viscosities, and that only the surface contribution is important; the system becomes therefore equivalent to a real two-dimensional system.)

In the limit of small surface viscosities, $\eta_s \to 0$, equivalent to $\kappa^{-1} \to 0$, the drag force due to the thin surface layer does not tend to zero. Indeed, even if the bidimensional viscous force vanishes, the surface pressure gradient does not vanish and tends to a finite value; this is the origin of a finite bidimensional force. More precisely, the value of the bidimensional force is equal to the drag force due to the subphase, as already pointed out by Stone & Ajdari (1998). However, it is important to notice that this limit simultaneously supposes $\eta_s = 0$ and the incompressibility of the flow. In practice, it corresponds to a monolayer, sufficiently dilute that the surface viscosity is negligible but sufficiently concentrated that the flow field can always be considered as incompressible. This limit does not allow one to extrapolate to the case of the disk translating at the free surface of a subphase, in the absence of any adsorbed monolayer, because the Stokes equations do not reduce to the zero shear stress condition of a free interface, even when $\eta_s = 0$. This means that the bulk flows are different in the presence and in the absence of a monolayer.

2.2.4. *Incompressibility criterion*

The surfactant conservation equation $\nabla_s \cdot (\Gamma \boldsymbol{u}_s) = 0$, where Γ is the surface density, gives an order of magnitude of $\nabla_s \cdot \boldsymbol{u}_s$:

$$\nabla_s \cdot \boldsymbol{u}_s \approx -\frac{1}{\Gamma} \boldsymbol{u}_s \cdot \nabla_s \Gamma = \frac{1}{E} \boldsymbol{u}_s \cdot \nabla_s \Pi_s \tag{2.21}$$

where $E = \Gamma \partial \Pi_s / \partial \Gamma$ is the Gibbs elasticity of the monolayer. Using (2.16), the surface pressure gradient can be estimated by considering the surface flow as incompressible. The monolayer can then be considered as incompressible if

$$\nabla_s \cdot \boldsymbol{u}_s \ll \frac{U}{R} \tag{2.22}$$

which is equivalent to

$$E \gg \frac{\eta R U}{h}. \tag{2.23}$$

2.3. *Gibbs monolayer*

A compressible surface layer has two viscosities: the shear viscosity η_s and the dilational viscosity η_d associated with the dilational rate of the area. In order to describe the experiments performed with the SDS solution, we assume that the surface layer is formed by soluble molecules and that the exchanges between the bulk and the interface are instantaneous so that the surface is always at equilibrium with the bulk and that the surface pressure is uniform. In § 3.3, we discuss in detail the various time scales associated with the disk displacement and to the surface–bulk exchange. There is then a flux of surfactant molecules from the surface to the bulk, so that the surface layer is necessarily compressible.

2.3.1. *Velocity field*

For a compressible monolayer, the Stokes equation reads

$$\eta_s \nabla_s^2 \boldsymbol{u}_s + \eta_d \nabla_s (\nabla_s \cdot \boldsymbol{u}_s) - \nabla_s \Pi_s + \boldsymbol{\sigma}_t = \boldsymbol{0}. \tag{2.24}$$

The shear stress is still given by (2.5) and the surface pressure is uniform, so that, for a soluble compressible monolayer,

$$\eta_s \nabla_s^2 \boldsymbol{u}_s + \eta_d \nabla_s (\nabla_s \cdot \boldsymbol{u}_s) - \frac{h}{2} \nabla_s P - \eta \frac{\boldsymbol{u}_s}{h} = \boldsymbol{0}, \tag{2.25}$$

with the same boundary conditions as for an incompressible monolayer. Here also, the symmetry of the problem imposes the angular variation of the surface velocity $\boldsymbol{u}_s$:

$$\boldsymbol{u}_s = U \left| \begin{array}{l} f(r)\cos\theta \\ -g(r)\sin\theta. \end{array} \right. \tag{2.26}$$

We calculate respectively the curl and the divergence of the velocity field; using the relation (2.7) between $\nabla_s^2 P$ and $\nabla_s \cdot \boldsymbol{u}_s$, we obtain

$$(\nabla_s^2 - \kappa^2) \nabla_s \times \boldsymbol{u}_s = \boldsymbol{0}, \tag{2.27a}$$

$$(\nabla_s^2 - \tilde{\kappa}^2) \nabla_s \cdot \boldsymbol{u}_s = 0 \quad \text{with} \quad \tilde{\kappa}^2 = \frac{4\eta}{h(\eta_s + \eta_d)}. \tag{2.27b}$$

Both the divergence and the curl of the velocity decay to zero at infinity and therefore

$$\nabla_s \times \boldsymbol{u}_s = B_1 K_1(\kappa r) U \sin\theta \, \boldsymbol{e}_z, \tag{2.28a}$$

$$\nabla_s \cdot \boldsymbol{u}_s = B_2 K_1(\tilde{\kappa} r) U \cos\theta, \tag{2.28b}$$

where B_1 and B_2 are two integration constants.

2.3.2. *Bulk pressure*

The bulk pressure satisfies (2.7). For $r < R$, the velocity is constant and equal to $\boldsymbol{U}$, so that its divergence vanishes, and for $r > R$ the velocity divergence is given by (2.28*b*). The bulk pressure then satisfies the following relations:

$$\left. \begin{array}{rl} \nabla_s^2 P = 0 & \text{for} \quad r < R, \\ \nabla_s^2 P = \dfrac{6\eta}{h^2} B_2 U K_1(\tilde{\kappa} r)\cos\theta & \text{for} \quad r > R. \end{array} \right\} \tag{2.29}$$

The equations for the velocity and the pressure are now decoupled, and, as in the insoluble case, it is possible to find a solution of the form (2.26) for $\boldsymbol{u}_s$ and of the form $h(r)\cos\theta$ for $P(r)$. The explicit derivation is rather tedious and is not presented here; the expressions for the velocity and of the pressure are given in Appendix B.

2.3.3. *Total force on the disk*

As in the incompressible case, the force acting on the disk has two origins. The drag force due to the subphase is

$$\boldsymbol{F}_{\text{sub.}} = \pi R^2 \boldsymbol{\sigma}_t = -\pi R^2 \left(\frac{\eta}{h} \boldsymbol{U} + \frac{h}{2} \nabla_s P \right) \tag{2.30}$$

and the force due to the thin surface layer is $\boldsymbol{F}_{\text{surf.}} = \int_0^{2\pi} R(\sigma_{rr}\boldsymbol{e}_r + \sigma_{r\theta}\boldsymbol{e}_\theta)\,\mathrm{d}\theta$. The transverse component of the stress is similar to that of incompressible monolayers and the radial component is $\sigma_{rr} = 2\eta_s \partial u_{sr}/\partial r + (\eta_d - \eta_s)\nabla_s \cdot \boldsymbol{u}_s$. Using the expressions given in Appendix B, we obtain

$$\boldsymbol{F}_{\text{tot.}} = -\pi R^2 \frac{\eta \boldsymbol{U}}{h} \left(8 \frac{K_2(\tilde{\kappa}R)K_2(\kappa R)}{K_0(\tilde{\kappa}R)K_2(\kappa R) + 4K_2(\tilde{\kappa}R)K_0(\kappa R)} \right). \tag{2.31}$$

In the limit of vanishing viscosities ($\eta_s, \eta_d \to 0$) the two-dimensional force due to the thin surface layer vanishes (unlike in the case of a compressible monolayer) as there is no surface pressure gradient. More precisely

$$\lim_{\eta_s, \eta_d \to 0} \boldsymbol{F}_{\text{tot.}} = \lim_{\eta_s, \eta_d \to 0} \boldsymbol{F}_{\text{sub.}} = -\tfrac{8}{5}\pi R^2 \frac{\eta \boldsymbol{U}}{h}. \tag{2.32}$$

In this limit, the hydrodynamic equations reduce to a vanishing shear stress at a free surface. Consequently, although the lubrication approximation may be no longer valid in the limit of small viscosities†, we believe that the limiting value of the force (2.32) is the drag force for a pure subphase:

$$\boldsymbol{F}_{\text{water}} = -\tfrac{8}{5}\pi R^2 \frac{\eta \boldsymbol{U}}{h}. \tag{2.33}$$

This result is confirmed by the direct calculation of the force, presented in Appendix C, in the singular‡ configuration of a disk overlying a subphase in the absence of any monolayer. In the limit of small screening length (still with the constraint $h \ll \kappa^{-1}$ to be able to use the lubrication approximation), the asymptotic behaviour of the bidimensional force is

$$\boldsymbol{F}_{\text{surf.}} = -\tfrac{8}{5}\pi R^2 \frac{\eta \boldsymbol{U}}{h} \left(\frac{1}{\kappa R} + \frac{1}{\tilde{\kappa} R} \right) \tag{2.34}$$

and the force scales as

$$\boldsymbol{F}_{\text{surf.}} = -R \left(\frac{\eta \eta_s}{h} \right)^{1/2} \boldsymbol{U} \propto -R\eta_s \frac{\boldsymbol{U}}{\kappa^{-1}}. \tag{2.35}$$

The monolayer of viscosity η_s exerts a viscous drag on the perimeter R of the disk with a velocity gradient U/κ^{-1}. Indeed, the variation of the surface velocity occurs over a distance $\kappa^{-1} \propto (\eta_s)^{1/2}$. It is interesting to notice that the velocity gradient increases with a decreasing surface viscosity, as shown in Appendix B, and diverges in the limit of $\eta_s = 0$.

† In this limit, the variation of the velocity occurs over distances κ^{-1} and $\tilde{\kappa}^{-1}$, which become smaller than h.

‡ The shear stress $\boldsymbol{\sigma}_t$ vanishes at the free interface and has a finite constant value on the disk, so that $\boldsymbol{\sigma}_t$ is discontinuous at $r = R$.

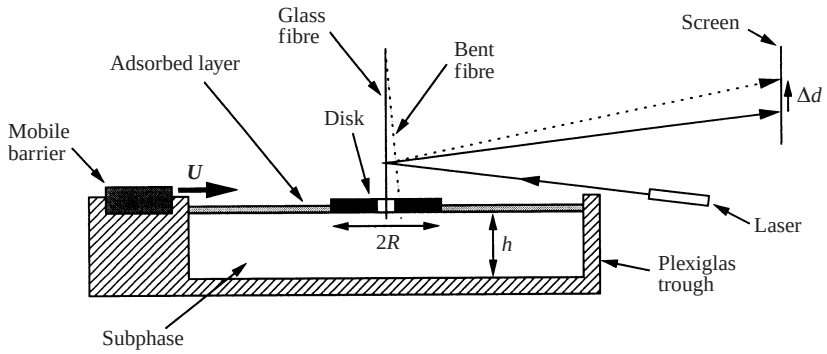

FIGURE 2. Experimental two-dimensional viscometer: when the trough moves, the subphase drags the disk, which bends the glass capillary. The deviation $\Delta d(\boldsymbol{U})$, proportional to the bending of the fibre, is measured on a distant screen.

3. Viscosity measurements

In this section, we first present the experimental device, the calibration of the force sensor and the experimental results. Then the comparison with the predicted force allows us to obtain the values of the surface viscosities.

3.1. *Experimental device*

The experimental device is sketched on figure 2. It is made of a Plexiglas trough (of depth 10 mm, width 112 mm and length 212 mm). The trough is linked to the mobile barrier of a commercial Langmuir trough (Lauda FW1), and can be moved at velocity $\boldsymbol{U}$ ($0.18\,\mathrm{mm\,s^{-1}} < U < 1.15\,\mathrm{mm\,s^{-1}}$). The trough is filled with purified water (Millipore system), to get a depth h ($2\,\mathrm{mm} < h < 8\,\mathrm{mm}$). A thin disk of radius R ($10\,\mathrm{mm} < R < 25\,\mathrm{mm}$), cut in a poly(ethylene-terephthalate) film, lies at the air–water interface. The disk has a tiny hole in its centre; a thin vertical glass capillary of radius $r = 30\,\mu\mathrm{m}$ is used as a force sensor. The upper end of the capillary is clamped in a fixed position and the lower end is inserted in the disk hole. The motion of the trough induces a drag of the water subphase on the disk, and a bending of the capillary as shown on figure 2. A laser beam is pointed at the capillary and its reflection is observed on a distant screen. The deviation of the laser spot on the screen is proportional to the bending of the capillary and thus to the total drag force acting on the disk. Before each experiment, the trough and the disk are washed with pure water. The adsorbed polymer (polyoxyethylene oxide) or surfactant (stearic acid) monolayer is obtained by solution of the product in chloroform (Merck pro analysi), and then spreading it onto pure water using a micro-syringe. After deposition, we wait for the evaporation of the spreading solvent. For each measurement of the deviation Δd, the disk is initially at one end of the trough; the trough is slowly accelerated until it reaches a constant velocity $\boldsymbol{U}$. After an inertial regime, the deviation of the spot stabilizes at a constant value. This value is measured as the disk goes through the centre of the trough. For each velocity, we also measure the deviation $-\Delta d$ corresponding to the experiment with the opposite velocity $-\boldsymbol{U}$ to increase the precision of the measurement and to avoid any offset problem. All experiments are performed at room temperature $T = 20 \pm 2\,^{\circ}\mathrm{C}$.

These experimental conditions correspond well to the assumptions made in the theoretical description:

we reach a well-defined stationary state;

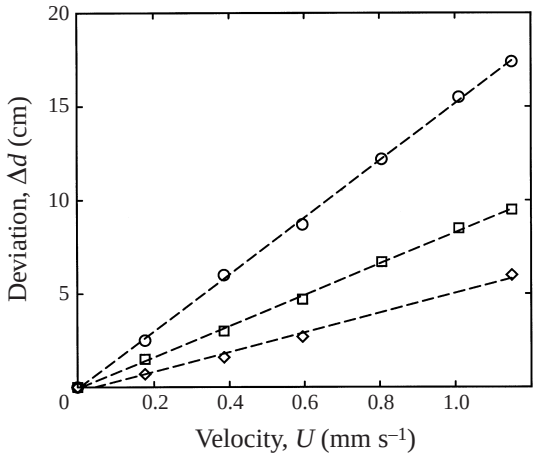

FIGURE 3. Influence of the subphase depth h on the deflection $\Delta d(\boldsymbol{U})$, $R = 25\,\text{mm}$, pure water: ○, $h = 2\,\text{mm}$; □, $h = 4\,\text{mm}$; ◇, $h = 8\,\text{mm}$; – – –, linear fit.

the depth of the water subphase is indeed smaller than the radius of the disk, since in most of the experiments, $h = 4\,\text{mm}$ and $R = 25\,\text{mm}$, so that $h/R < 0.2$, and from Stone & Ajdari (1998), we know that the lubrication approximation is accurate;

the inertial terms can be neglected compared to the viscous terms in the hydrodynamic description, so that linear hydrodynamics is appropriate. Indeed, we have

$$\frac{\|\rho \boldsymbol{v} \cdot \nabla \boldsymbol{v}\|}{\|\eta \nabla^2 \boldsymbol{v}\|} \approx \frac{\rho U h^2}{\eta R} \approx \frac{1}{10} \tag{3.1}$$

with ρ the liquid volumic mass.

3.2. *Calibration with pure water*

As already pointed out in the previous section, the total drag force acting on the disk has two contributions: that of the subphase (water) and of the monolayer. It is important to determine the two contributions independently; we therefore measure the force exerted on the disk by a pure water subphase in the absence of any adsorbed layer. Another crucial reason for the measurement with pure water is the calibration of the glass fibre: it being not of homogeneous radius it is difficult both to calculate and to calibrate its bending constant. Using (2.32), we know for each velocity the corresponding force, so that each deviation $\Delta d(\boldsymbol{U})$ can be associated with a value of the force.

Figure 3 shows the deviation Δd as a function of the velocity $\boldsymbol{U}$ of the trough, obtained with a disk of radius $R = 25\,\text{mm}$, for three values of h. We observe the excellent linearity of the response and the decrease of the deviation (and thus of the force) with increasing depth h. In figure 4, the deviation of the spot is plotted as a function of R^2U/h to check the variation with the various parameters R, h, U; we obtain a good agreement with the theoretical prediction. The experiments were performed with four different sizes of disk, three values of the subphase depth and five velocities. The order of magnitude of the measured forces is 10^{-7}–10^{-6} N.

The linearity observed on figure 4 indicates that the effects of the finite size of the trough are negligible, since important finite size effects would induce higher drag forces on the larger disks, which is not the case in our measurements. Another way to estimate the importance of the finite size effect is to study theoretically the velocity

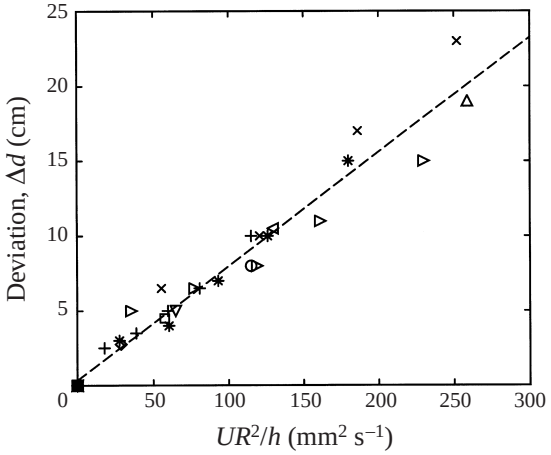

FIGURE 4. Deflection Δd as a function of UR^2/h, pure water. $R = 10$ mm: ○, $h = 1$ mm; □, $h = 2$ mm; ◇, $h = 4$ mm. $R = 15$ mm: △, $h = 1$ mm; ◁, $h = 2$ mm; ▽, $h = 4$ mm. $R = 20$ mm: ▷, $h = 2$ mm; +, $h = 4$ mm. $R = 25$ mm: ×, $h = 2$ mm; *, $h = 4$ mm; – – –, linear fit.

field. In Appendix C, we calculate the average velocity for an infinite system and we see that, for a disk of $R = 25$ mm, the velocity is $V_\theta = -0.08\,U$ at $r = 55$ mm, which is the distance to the walls in the experimental device. This gives an idea of the difference between the experimental and the theoretical velocity fields. We also solved the hydrodynamic equations in a steady state but assuming that the velocity vanishes at a distance L from the centre. This is only approximate but it gives a logarithmic dependence on the size of the system and leads to a maximum correction of about 10% compared to a system of infinite size.

3.3. *Soluble surfactant: SDS*

3.3.1. *Experimental results*

In order to estimate the sensitivity of the experimental device, it is interesting to study solutions of SDS, for which the surface viscosity has been already measured by Petkov *et al.* (1996) and Poskanzer & Goodrich (1975*b*). With two different experimental techniques, both groups find a surface viscosity around 2×10^{-6} Pa m s. In our experiment, water is replaced by a concentrated solution of SDS ($c = 10\,\mathrm{g\,l^{-1}} \approx 4$ c.m.c., the critical micellar concentration of SDS being c.m.c. $= 2.4\,\mathrm{g\,l^{-1}}$). The subphase has almost the same viscosity as water (the viscosity is increased by less than 5%) and is covered by an adsorbed layer of soluble surfactants. The concentration of the solution is the same as in Petkov *et al.* (1996), which allows comparison of the results. The other reason to study concentrated solutions is that the surface is at instantaneous equilibrium with the bulk; the exchanges of surfactants are fast enough to ensure a constant surface concentration. Indeed the characteristic time associated with the disk displacement ($T = R/U$) is roughly 25 s, which is higher than the characteristic time associated with the diffusional exchanges between the bulk and the interface (0.4 s for a SDS solution of $c = 1.5\,\mathrm{g\,l^{-1}}$, from MacLeod & Radke 1993). For each experiment, we prepared and used fresh solutions to avoid the hydrolysis of SDS into dodecanol. The time scale of this hydrolysis is of order of one day (Mysels 1986), while the measurements are performed over less than one hour.

Figure 5(*a*) shows the deviations of the spot position, as a function of the velocity, with a disk of radius $R = 25$ mm and with three different depth values. As in the case

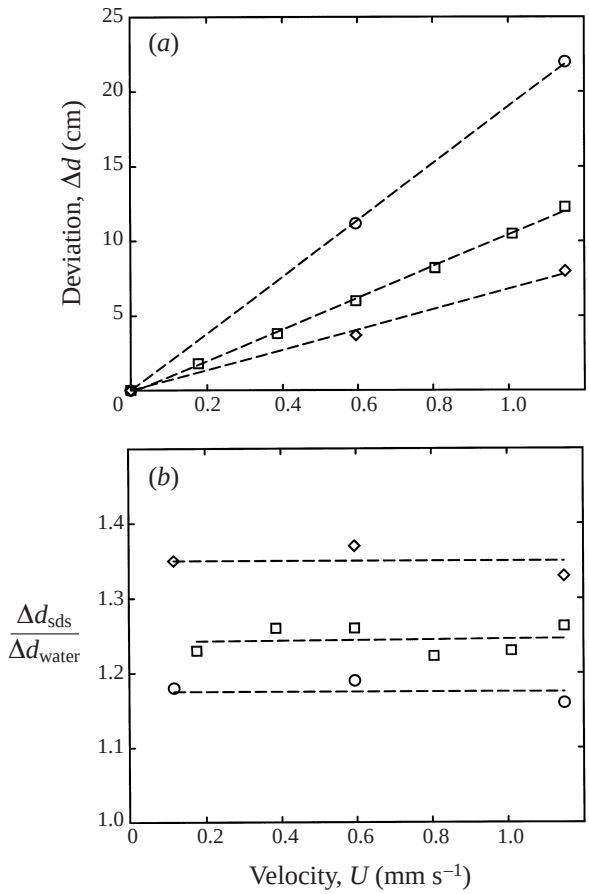

FIGURE 5. Influence of SDS solution on the deflection for different depth ($R = 25\,\text{mm}$, $c = 10\,\text{g}\,\text{l}^{-1}$): ○, $h = 2\,\text{mm}$; □, $h = 4\,\text{mm}$; ◇, $h = 8\,\text{mm}$; – – –, linear fit. (*a*) Deflection $\Delta d(\boldsymbol{U})$ for different subphase depth; (*b*) comparison between the deflection for SDS and for pure water.

of pure water, we checked the linearity of the response and the decrease of the force, when h increases. On figure 5(*b*), the deviation obtained with SDS is compared to that found with pure water. The deviation is increased by 18% to 35%, depending on the depth h, as water is replaced by the SDS solution. This increase is much larger than the small increase due to the change in the bulk viscosity, and is the signature of surface viscosity. The ratio of the deviations for the SDS solution and pure water is mostly independent of the velocity.

3.3.2. *Interpretation*

As the exchanges between the bulk and the surface are sufficiently fast to ensure a constant value of the surface pressure, the surface layer of surfactants can be described by the theoretical model of a compressible and soluble layer, developed in § 2.3. The ratio of deviations of the spot directly gives the ratio of the theoretical forces on the disk, calculated in the presence and in the absence of adsorbed layer:

$$\frac{\Delta d_{\text{SDS}}}{\Delta d_{\text{water}}} = \frac{F_{\text{tot.}}}{F_{\text{water}}} = \frac{5}{8}\left(\frac{8K_2(\tilde{\kappa}R)K_2(\kappa R)}{K_0(\tilde{\kappa}R)K_2(\kappa R) + 4K_2(\tilde{\kappa}R)K_0(\kappa R)}\right). \tag{3.2}$$

The force ratio is independent of the velocity, in agreement with the results of figure 5(*b*). The monolayer has two independent surface viscosities and we perform only one measurement. As Petkov *et al.* (1996), we will assume that one of the viscosities is known, for example η_d, and we deduce the other viscosity from the experimental results. Kao *et al.* (1992) give 3×10^{-8} Pa m s for the dilational viscosity. Using this value, the results of figure 5(*b*) together with (3.2) let us obtain the shear viscosity. For all the experiments (with three different depths), we find the same value:

$$\eta_s = 2.6 \times 10^{-6} \text{ Pa m s}. \tag{3.3}$$

This value is close to that given in Petkov *et al.* (1996) and Poskanzer & Goodrich (1975*b*). It is important to notice that the choice of η_d is not crucial, because the ratio of the spot deviations varies only very weakly with η_d, as already noticed by Danov *et al.* (1995). If we assume, that the two viscosities are of the same order of magnitude $\eta_s \approx \eta_d$, we find $\eta_s = 2.3 \times 10^{-6}$ Pa m s, which is close to the previous value. This range of viscosities corresponds to $\kappa R \approx 10$ and, in the limit of large κR, the force ratio increases as the square of the depth h:

$$\frac{F_{\text{tot.}}}{F_{\text{water}}} - 1 \approx \left(\frac{8}{5} \frac{1}{\kappa R} + \frac{2}{5} \frac{1}{\tilde{\kappa} R} \right) \propto \sqrt{h}. \tag{3.4}$$

This dependence also agrees with the results of figure 5(*b*).

3.4. *Insoluble monolayers*

In this subsection, we study monolayers of stearic acid ($H_{35}C_{17}$-COOH), and of a telechelic polyethylene oxide (PEO). The stearic acid was purchased from Sigma and the end-capped PEO ($H_{25}C_{12}$-O-$(CH_2$-CH_2-$O)_{800}$-$C_{12}H_{25}$) samples were synthesised by G. Beinert and F. Isel (ICS, Strasbourg): commercial PEO with terminal OH groups, with narrow mass distribution, was purchased and then functionalized. The synthesis details can be found in Maitre (1997) along with the characterization.

For such insoluble monolayers, there is no exchange with the bulk, and according to (2.23), the monolayer can be considered as incompressible, if $E \gg \eta R U / h$. With our experimental conditions, this criterion becomes $E \gg 10^{-2}$ mN m^{-1}, which is always fulfilled, as soon as a small quantity of surfactant is spread at the air–water interface (see Gaines 1966 and Poskanzer & Goodrich 1975*a* for the stearic acid isotherm and Barentin, Muller & Joanny 1998 for the end-capped PEO isotherm).

3.4.1. *Results*

Figure 6 shows the first results obtained with the two surfactants and the ratio of spot deviations $\Delta d(\text{monolayer})/\Delta d(\text{water})$ obtained at different surface densities. All the measurements are performed with one disk and one depth. For small surface densities, the ratios of deviations, for the two surfactants, are close. Indeed the increase of the deviation, compared to the deviation obtained with pure water, is roughly 25%. For higher surface densities, the ratio increases and depends on the nature of the surfactant. For dense monolayers of stearic acid, the drag force becomes larger than with PEO monolayers. Finally, as in the case of the SDS solutions, the ratios of the spot deviations are independent of the velocity.

3.4.2. *Interpretation*

The insoluble surfactant monolayers are described by the theoretical model of incompressible layers, developed in § 2.2. The ratio of the deviations corresponds to

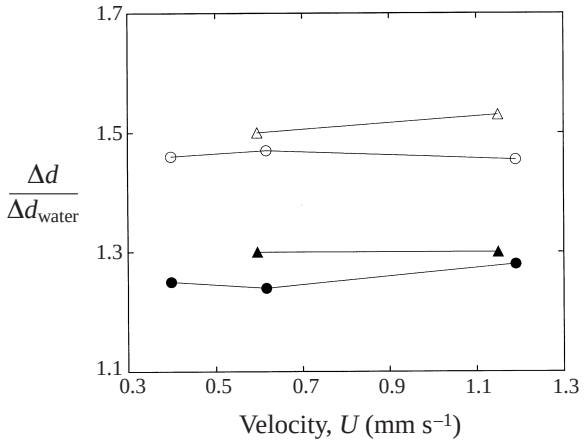

FIGURE 6. Ratio between the deflections for insoluble monolayers and for pure water. $R = 20$ mm, $h = 4$ mm and stearic acid: •, 36 Å^2/molecule; ○, 20 Å^2/molecule. $R = 25$ mm, $h = 4$ mm and PEO: ▲, 27 Å^2/monomer; △, 17 Å^2/monomer.

the ratio of the theoretical forces:

$$\frac{\Delta d_{\text{monolayer}}}{\Delta d_{\text{water}}} = \frac{F_{\text{tot.}}}{F_{\text{water}}} = \frac{5}{4}\frac{K_2(\kappa R)}{K_0(\kappa R)}. \tag{3.5}$$

In the limit of small viscosity, $\eta_s \to 0$, the ratio of the forces (3.5) tends to $\frac{5}{4}$, and not to 1, because there is a remaining bidimensional force due to the surface pressure gradient, that does not vanish. This predicted value of $\frac{5}{4}$ describes well the experimental results obtained at small surface densities. However we cannot estimate the surface viscosity, because the bidimensional viscous force is negligible compared to the bidimensional force due to the pressure gradients. At higher surface densities, when the ratio of the deviations increases and becomes larger than this limit value of $\frac{5}{4}$, it is possible, using (3.5), to determine the surface viscosities. We obtain, for the PEO monolayer at 17Å^2/monomer,

$$\eta_s = 1.6 \times 10^{-6}\ \text{Pa m s} \tag{3.6}$$

and for the stearic acid monolayer at 20 Å^2/molecule

$$\eta_s = 5 \times 10^{-7}\ \text{Pa m s}. \tag{3.7}$$

This last value is smaller than that measured by Poskanzer & Goodrich (1975*a*). In this range of surface densities, the surface pressure of monolayers of stearic acid, increases strongly (Gaines 1966). As we could not measure the surface pressure, it is possible that the uncertainty due to the spreading is at the origin of this discrepancy between the two values.

4. Concluding remarks

In this paper, we have presented a new and original two-dimensional viscosimeter, and the hydrodynamic calculations used to obtain the surface viscosities from the measurements. We have developed different hydrodynamic models of insoluble and soluble (with no surface pressure gradient) monolayers and to describe the experimental systems. Since we have no absolute calibration of the force sensor, we had to

calculate the drag force acting on the disk in the absence of any adsorbed surface layer; we found an expression higher by a factor $\frac{8}{5}$ than the force resulting from a simple shear (Stone & Ajdari 1998).

The theoretical predictions describe well the drag forces obtained with the insoluble monolayers of surfactants at small surface densities and give an estimation of the surface viscosities at higher densities. We have also performed measurements with other insoluble polymer monolayers (Poly(vinyl-acetate) and Poly(dimethyl-siloxane) in the presence of SDS). In all cases, the measured force at low density is of order 25% larger than the value obtained in the absence of monolayer in agreement with our predictions. The absolute value of the surface shear viscosity is however too low to be measured quantitatively for these systems. In the case of the solutions of SDS, the calculations allow one to determine the surface viscosity; the value is in good agreement with previous studies (Petkov *et al.* 1996; Poskanzer & Goodrich 1975*b*).

In order to study more systematically adsorbed monolayers such as PEO or stearic acid, it is necessary to improve the experimental device by combining the viscosity measurement with a surface pressure measurement. Another improvement would be to use a capillary with a well-defined bending constant, in order to check experimentally the expression for the drag force in the case of pure water in the absence of monolayer. In order to analyse the influence of the disk radius and of the finite size of the trough, it would also be useful to visualize the surface velocity field and to compare it with the theoretical field calculated for an infinite system. Finally, it would be interesting to do the same experiment at finite frequency in order to measure the viscoelasticity of the monolayers. The steady state results can still be used if the frequency is smaller than both the surface viscoelastic relaxation time τ_R^{-1} and the diffusion time of vorticity over the bulk liquid film $\eta/(h^2\rho)$.

We are grateful to F. Isel, G. Beinert and J. François (ICS, Strasbourg, France) who have provided the telechelic PEO. We also thank P. Woehl and G. Bouchet (IMF, Strasbourg, France) for constructive discussions and P. Muller (ICS, Strasbourg, France) for his help in the experiments.

Appendix A. Bulk pressure gradients

In this Appendix, we study the order of magnitude of the various derivatives of the pressure, in the lubrication approximation. From the Stokes equations (2.1*a*, *b*), we know that

$$\frac{\partial P}{\partial x} \sim \frac{\eta U}{h^2}, \quad \frac{\partial P}{\partial z} \sim \frac{\eta v_z}{h^2}. \tag{A 1}$$

In the lubrication approximation, v_z is negligible compared to U, which implies that $\partial P/\partial z$ is also negligible compared to $\partial P/\partial x$. The incompressibility of the flow $\boldsymbol{\nabla}\cdot\boldsymbol{v} = 0$ leads to

$$\frac{v_z}{h} \simeq \frac{U}{R} \tag{A 2}$$

with $h \ll R$. From (A 1), we can estimate the second derivatives of the pressure:

$$\frac{\partial^2 P}{\partial x^2} \simeq \eta \frac{U}{h^2 R}, \quad \frac{\partial^2 P}{\partial z^2} \simeq \eta \frac{v_z}{h^3}. \tag{A 3}$$

The relation (A 2) imposes that U/h^2R and v_z/h^3 are of the same order of magnitude. This means that $\partial^2 P/\partial x^2$ and $\partial^2 P/\partial z^2$ are also of the same order of magnitude.

Appendix B. Velocity and pressure fields of Gibbs soluble monolayer

B.1. *Velocity field*

The surface velocity has the following expression:

$$\boldsymbol{u}_s = U \begin{vmatrix} f(r)\cos\theta \\ -g(r)\sin\theta, \end{vmatrix} \tag{B 1}$$

with

$$f(r) = -\frac{B_3}{r^2} - \frac{B_1}{r}\frac{K_1(\kappa r)}{\kappa r} - \frac{B_2}{\tilde{\kappa}}\left(K_0(\tilde{\kappa}r) + \frac{K_1(\tilde{\kappa}r)}{\tilde{\kappa}r}\right) \tag{B 2}$$

and

$$g(r) = \frac{B_3}{r^2} + \frac{B_2}{r}\frac{K_1(\tilde{\kappa}r)}{\tilde{\kappa}r} + \frac{B_1}{\kappa}\left(K_0(\kappa r) + \frac{K_1(\kappa r)}{\kappa r}\right). \tag{B 3}$$

The integration constants are expressed as functions of κ, $\tilde{\kappa}$ and R:

$$B_1\frac{K_0(\kappa R)}{\kappa} = \frac{8K_0(\kappa R)K_2(\tilde{\kappa}R)}{K_0(\tilde{\kappa}R)K_2(\kappa R) + 4K_2(\tilde{\kappa}R)K_0(\kappa R)}, \tag{B 4}$$

$$B_2\frac{K_0(\tilde{\kappa}R)}{\tilde{\kappa}} = \frac{2K_2(\kappa R)K_0(\tilde{\kappa}R)}{K_0(\tilde{\kappa}R)K_2(\kappa R) + 4K_2(\tilde{\kappa}R)K_0(\kappa R)} \tag{B 5}$$

and

$$B_3 = -\frac{R^2}{2}\left(B_1\frac{K_2(\kappa R)}{\kappa} + B_2\frac{K_2(\tilde{\kappa}R)}{\tilde{\kappa}}\right). \tag{B 6}$$

B.2. *Influence of the surface viscosity on the velocity field*

On figure 7(a), we plot the surface velocity $u_{s,\theta}(r, \theta = \pi/2)$ as a function of r, for three values of the shear surface viscosity. Close to the disk the velocity is negative, the flow has the same direction as $\boldsymbol{U}$, and far from the disk the velocity becomes positive, which is a consequence of the flux conservation. The velocity gradients increase when the surface viscosity decreases. If the monolayer is less viscous, the disk motion induces a velocity field that decays faster with the distance. On figure 7(b), we plot the radial surface velocity $u_{s,r}(r, \theta = 0)$, for three values of the surface shear viscosity.

B.3. *Bulk pressure*

For $r < R$, the pressure is given by

$$P(r,\theta) = -\frac{3\eta}{h^2}B_2\frac{K_0(\tilde{\kappa}R)}{\tilde{\kappa}}rU\cos\theta \tag{B 7}$$

and for $r > R$

$$P(r,\theta) = -\frac{3\eta}{h^2}\frac{B_2}{\tilde{\kappa}}U\left(2\frac{R}{r}\frac{K_1(\tilde{\kappa}R)}{\tilde{\kappa}} - 2\frac{K_1(\tilde{\kappa}r)}{\tilde{\kappa}} + \frac{R^2}{r}K_0(\tilde{\kappa}R)\right)\cos\theta. \tag{B 8}$$

Appendix C. Force in the absence of a surface layer

C.1. *Bulk pressure*

For $r < R$, the velocity is constant, equal to $\boldsymbol{U}$, so that its divergence vanishes and (2.7) becomes

$$\nabla_s^2 P = 0. \tag{C 1}$$

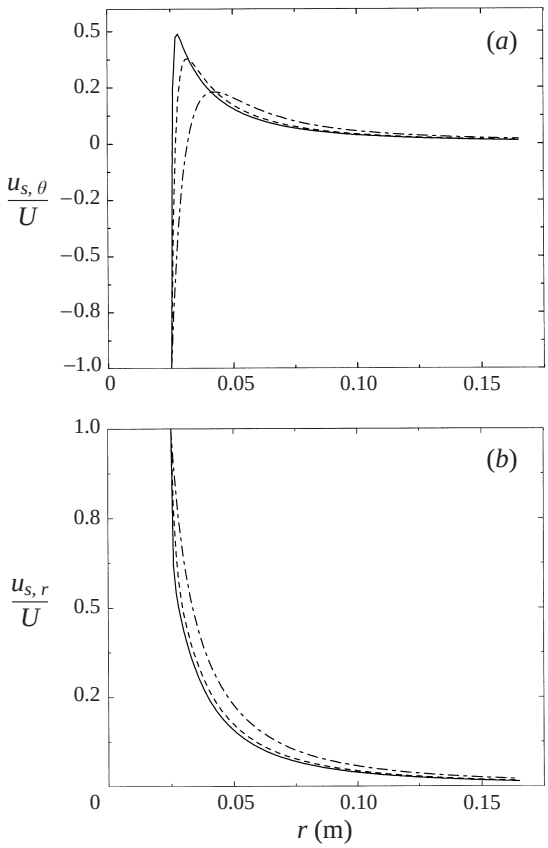

FIGURE 7. Effect of the surface shear viscosity on the velocity of the Gibbs monolayer ($\eta_s = \eta_d$, $R = 25$ mm): $\eta_s = 10^{-5}$ Pa m s (—·—), $\eta_s = 10^{-6}$ Pa m s (– – –), $\eta_s = 10^{-7}$ Pa m s (——). (*a*) $u_{s,\theta}(r, \theta = \pi/2)$ as a function of r; (*b*) $u_{s,r}(r, \theta = 0)$ as a function of r.

The pressure varies thus as

$$P(r, \theta) = ArU \cos\theta \tag{C 2}$$

where A is a constant. For $r > R$, the shear stress (2.5) vanishes at the free surface, so that

$$\nabla_s P = -\frac{2\eta}{h^2}\boldsymbol{u}_s. \tag{C 3}$$

Taking the divergence of this equation and comparing with (2.7), we obtain

$$\nabla_s^2 P = 0, \quad \nabla_s \cdot \boldsymbol{u}_s = 0. \tag{C 4}$$

The pressure field is therefore given by

$$P(r, \theta) = \frac{B}{r} U \cos\theta \tag{C 5}$$

where B is an other constant related to A by the continuity of the pressure at $r = R$, $B = AR^2$.

C.2. *Average velocity*

We define the average velocity, as in § 2.1, by

$$\boldsymbol{V}(r,\theta) = \frac{1}{h}\int_0^h \boldsymbol{v}_{\shortparallel}(r,\theta,z)\,\mathrm{d}z = -\frac{h^2}{12\eta}\nabla_s P + \frac{\boldsymbol{u}_s}{2}. \tag{C 6}$$

For $r < R$, $\boldsymbol{u}_s = \boldsymbol{U}$ and for $r > R$ the velocity is proportional to the pressure gradient (C 3). Using the expressions for the pressure, we find

$$\boldsymbol{V} = \begin{cases} \left(-\dfrac{h^2}{12\eta}A + \dfrac{1}{2}\right)\boldsymbol{U} & \text{for} \quad r < R \\ \dfrac{h^2}{3\eta}A\dfrac{R^2}{r^2}\,(\boldsymbol{U} + 2U\sin\theta\,\boldsymbol{e}_\theta) & \text{for} \quad r > R. \end{cases} \tag{C 7}$$

To determine the constant A, we use the fact that the radial component of the average velocity V_r, associated with mass conservation, is continuous at $r = R$. In a finite system, this condition is equivalent to writing that the mass flux or flow through a plane perpendicular to the disk movement is zero: $\int_0^L \boldsymbol{V}(r, \frac{1}{2}\pi)\cdot\boldsymbol{e}_x\,\mathrm{d}r = 0$, where L is the size of the trough and $\boldsymbol{e}_x$ is the unit vector along $\boldsymbol{U}$. This condition implies

$$A = \frac{6}{5}\frac{\eta}{h^2}. \tag{C 8}$$

This result allows the determination of the pressure gradient under the disk and the shear stress on the surface using (2.5). We finally find that the drag force is

$$\boldsymbol{F}_{\text{water}} = -\tfrac{8}{5}\pi R^2\frac{\eta\boldsymbol{U}}{h}. \tag{C 9}$$

This is the same expression as found with a soluble surface layer, in the limit of vanishing surface viscosities. Using (C 8), we can express the average velocity as

$$\boldsymbol{V} = \begin{cases} \tfrac{2}{5}\boldsymbol{U} & \text{for} \quad r < R \\ \dfrac{2}{5}\dfrac{R^2}{r^2}\,(\boldsymbol{U} + 2U\sin\theta\,\boldsymbol{e}_\theta) & \text{for} \quad r > R. \end{cases} \tag{C 10}$$

The radial component of the average velocity V_r is continuous when $r = R$ as implied by the conservation of the mass flux. The transverse component V_θ is not associated with mass conservation. It is discontinuous in the lubrication approximation. In practice, with a finite but small surface viscosity there exists at the edge of the disk a thin boundary layer where the tangential velocity varies very rapidly. Our model is not able to describe correctly this fast variation.

REFERENCES

Abramowitz, M. & Stegun, I. 1984 *Handbook of Mathematical Functions*. Franckfurt: Verlag Harri Deutsch.

Barentin, C., Muller, P. & Joanny, J. 1998 Polymer brushes formed by end-capped poly(ethylene oxide) (PEO) at the air-water interface. *Macromolecules* **31**, 2198–2211.

Clegg, R. & Vaz, W. 1985 Translational diffusion of proteins and lipids in artificial lipid bilayer membranes. A comparison of experiment with theory. *Progress in Protein Lipid Interactions.* Elsevier.

Danov, K., Aust, R., Durst, F. & Lange, U. 1995 Influence of the surface viscosity on the hydrodynamic resistance and surface diffusivity of a large brownian particle. *J. Colloid Interface Sci.* **175**, 36–45.

EDWARDS, D., BRENNER, H. & WASAN, D. 1991 *Interfacial Transport Process and Rheology*. Butterworth-Heinemann.

EVANS, E. & SACKMANN, E. 1988 Translational and rotational drag coefficients for a disk moving in a liquid membrane associated with a rigid substrate. *J. Fluid Mech.* **194**, 553–561.

GAINES, G. 1966 *Insoluble Monolayers at Liquid–Gas Interfaces*. Interscience.

HAPPEL, J. & BRENNER, H. 1991 *Low Reynolds Number Hydrodynamics*. Kluwer.

HUGHES, B., PAILTHORPE, B. & WHITE, L. 1981 The translational and rotational drag on a cylinder moving in a membrane. *J. Fluid Mech.* **110**, 349–372.

KAO, R., EDWARDS, D. A., WASAN, D. & CHEN, E. 1992 Measurement of interfacial dilatational viscosity at high rates of interface expansion using the maximum bubble pressure method. *J. Colloid Interface Sci.* **148**, 247–256.

MACLEOD, C. A. & RADKE, C. J. 1993 A growing drop technique for measuring dynamic interfacial tension. *J. Colloid Interface Sci.* **160**, 435–448.

MAITRE, S. 1997 Études des solutions aqueuses de polymères poly(oxyéthylène) modifiés par des extrémités hydrophobes. PhD thesis, Université Louis Pasteur, Strasbourg, France.

MALHOTRA, A. & WASAN, D. 1988 In *Thin Liquid Films: Fundamentals and Applications* (ed. I. B. Ivanov). Surfactant Science Series 29. Marcel Dekker.

MANNHEIMER, R. & SCHECHTER, R. 1970 An improved apparatus and analysis for surface rheological measurements. *J. Colloid Interface Sci.* **32**, 195–211.

MYSELS, K. 1986 Surface tension of solutions of pure sodium dodecyl sulfate. *Langmuir* **2**, 423–428.

PETKOV, J., DANOV, K. & DENKOV, N. 1996 Precise method for measuring the shear surface viscosity of surfactant monolayers. *Langmuir* **12**, 2650–2653.

POSKANZER, A. & GOODRICH, F. 1975*a* A new viscometer of high sensitivity. ii. experiments with stearic acid monolayers. *J. Colloid Interface Sci.* **52**, 213–221.

POSKANZER, A. & GOODRICH, F. 1975*b* Surface viscosity of sodium dodecyl sulfate with and without added dodecanol. *J. Phys. Chem.* **79**, 2122–2126.

SAFFMAN, P. 1976 Brownian motion in thin sheets of viscous fluid. *J. Fluid Mech.* **73**, 593–602.

SAFFMAN, P. & DELBRUCK, M. 1975 Brownian motion in biological membranes. In *Proc. Natl Acad. Sci. USA* **72**, 311–313.

STONE, H. & AJDARI, A. 1998 Hydrodynamics of particles embedded in a flat surfactant layer overlying a subphase of finite depth. *J. Fluid Mech.* **369**, 151–173.

VAZ, W., STUMPEL, J., HALLMANN, D., GANBACORTA, A. & ROSA, M. D. 1987 Bounding fluid viscosity and translational diffusion in a fluid lipid bilayer. *Eur. Biophys. J.* **15**, 111–115.